SUPPLEMENTARY MATERIAL

Secondary Metabolites from *Lantana camara* L. Flowers Extract Exhibit *in vivo* Anti-urolithiatic Activity in Adult Wistar Albino Rats

Marwa I. Ezzat[1], Salsabeel N. El Gendy[1,*], Ahmed S. Saad[2], Walied S. Abdo[3], Aly M. EL Sayed[1] and Amira K. Elmotayam[1]

[1] Pharmacognosy Department, Faculty of Pharmacy, Cairo University, Kasr El-Ainy Street, Cairo 11562, Egypt

[2] Department of Pharmacology and Toxicology, Faculty of Pharmacy, Port Said University, Port Said, Egypt

[3] Department of Pathology, Faculty of Veterinary medicine, Kaferelsheik University, Kafrelsheikh 33516, Egypt

[*] Correspondence: E-mail: ph.salsabeel@hotmail.com Tel.: 00201118599904

Abstract

The present study aims at evaluating the potential of the ethanol extracts of *L. camara* leaves (LE), flowers (FlE), and roots (RE) in the treatment of renal calculi and characterizing the secondary metabolites in the active extract. The results revealed that the FlE had significantly reduced the levels of kidney parameters (calcium, creatinine, urea, and uric acid) against ethylene glycol (EG) injures, and restored the activity of the natural antioxidants; glutathione peroxidase (GPx), superoxide dismutase (SOD) and lipid peroxide malondialdehyde (MDA) to the normal level. In addition, FlE significantly attenuated iNOS tissue expression caused by EG. The results obtained in this study suggest the potential value of the *L. camara* L. flowers as an antiurolithiatic agent.

Keywords: *Lantana camara* L., HPLC-PDA-MS/MS, flavonoids, phenylethanoids, ethylene glycol, antiurolithiatic.

Materials and methods

Plant material and extraction

The different parts (leaves, flowers and roots) of *L. camara* L. were collected in September 2016, from the experimental station of medicinal, aromatic and poisonous plants, Department of Pharmacognosy, Faculty of Pharmacy, Cairo University. Prof. Abd-Halim Megaly, Professor of plant taxonomy in agriculture museum, authenticated the plant. A voucher specimen (30-10-2016) was placed in the Herbarium of Pharmacognosy Department, College of Pharmacy, Cairo University, Egypt. The leaves, flowers and roots of *L. camara* L. were air dried under normal environmental conditions and then subjected to size reduction to get coarse powder. The dried powders (700 g of leaves, 300 g of flowers, and 211 g of roots) were separately extracted with ethanol 70% by cold maceration until complete exhaustion. The ethanol extract of each organ was evaporated under reduced pressure at a temperature not exceeding 40 ºC to yield the corresponding extracts, viz., leaves (LE, 75.7 g), flowers (FlE, 128.3g) and roots (RE, 7.9 g).

HPLC-PDA-MS/MS

LC-PDA-MS analysis system consists of HPLC thermofingan (Thermo electron corporation, USA) and LCQ-Duo ion trap mass spectrometer with an ESI source (Thermo Quest). The separation was achieved using Zorbax Eclipse XDB-C18 reversed phase column (150 x 4.6 mm, 3.5 µm, Agilent, USA) as previously reported (Ghareeb et al. 2019).

In vivo antiurolithiatic activity

Experimental animals

Adult male Wistar rats weighting 150 - 200 g were housed in the Pharmacology and Toxicology animal facility, Faculty of Pharmacy, Port Said University. The rats were kept in groups at constant temperature (23 ± 2 ºC), humidity (55 ± 1%) and a light/dark (12/12 h) cycle. Animals were acclimatized for one week and allowed free access to water *ad libitum*. The study was performed in accordance to the guidelines of the Animal Research: Reporting of *in vivo* Experiments (ARRIVE) guidelines, developed by the National Center for the Replacement, Refinement and Reduction of Animals in Research (NC3Rs). The experimental protocol was approved by the Ethics Committee for Animal Experimentation of the Faculty of Pharmacy, Cairo University (Permit Number: MP 1881).

Experimental design

Rats were classified into 13 groups (7 animals, each) and were treated as follows: Group I control (saline feeding), groups II – V control animals that orally received cystone (400 mg/ kg), FlE (400 mg/ kg), RE (400 mg/ kg) and LE (400 mg/ kg) from the day 15th to 28th of the experiment. Group VI Calculi-induced, received 0.75% ethylene glycol in drinking water from the 1st to 28th day and were left untreated. Group VII Standard curative group received 0.75% ethylene glycol in drinking water from 1st to 28th day and received orally 400 mg/kg b.wt. standard drug cystone from day 15th to 28th. Groups VIII - XIII curative groups, received 0.75% ethylene glycol in drinking water from 1st to 28th day then received orally FlE (200 and 400 mg/kg b.wt.), RE (200 and 400 mg/kg b.wt.) and LE (200 and 400 mg/kg b.wt.), respectively from day 15th to 28th (Abdel-hady et al. 2018) (Bora & Singh 2019). At the end of the experiment, the rats were sacrificed under sodium pentobarbitone anesthesia according to the guidelines for euthanasia in the Guide for the Care and Use of Laboratory Animals (2011).

Tissue and serum samples preparation

Blood samples were obtained from the retro-orbital plexus using microcapillaries (Optilab, Berlin, Germany). The serum of each animal was separated through blood centrifugation at 3000 *g* for 5 min to measure biochemical parameters (serum calcium, creatinine, urea and uric acid).. The kidney was dissected into two portions, one was immersed in neutral buffer formalin for histopathology examination and the other was kept at – 20 °C for the antioxidant potential evaluation.

Biochemical analyses

The serum level of creatinine was assayed by colorimetric-kinetics method according to the instructions of Diamond diagnostic kits, Egypt. Urea and Uric acid were assayed utilizing end point method following the instructions of Spectrum diagnostic kit, Egypt. Calcium was measured using ion selective electrode method of electrolyte analysis system (Caretium, China).

Evaluation of the oxidative stress markers

Kidneys were homogenized in 2 ml cold buffer (50 mM potassium phosphate, pH 7.5, 1 mM EDTA) per g tissue, using tissue homogenizer. The kidney homogenate was

centrifuged at 4000 rpm for 15 min at 4^{o} C. The obtained supernatant was used for the determination of glutathione peroxidase, superoxide dismutase and lipid peroxidation.

To determine the lipid peroxidation, thiobarbituric acid reactive substances (TBARS) level was measured as malondialdehyde (MDA). The reaction mixture composed of 0.2 ml supernatant of 50% w/v kidney homogenate, 1 ml of thiobarbituric acid (25 mmol/L) was added and mixed well. The mixture was heated in boiling water bath for 30 min then cooled. The absorbance was measured at 534 nm. For measuring superoxide dismutase activity (SOD), 0.1 ml supernatant of 50% w/v kidney homogenate was mixed with 1 ml of working reagents (phosphate buffer pH 8.5, nitroblue tetrazolium and NADH mixed in ratio of 10+1+1 ml). The reaction was initiated by the addition of 0.1 ml of phenazine methosulphate. An increase in the absorbance at 560 nm was recorded for 5 min at 25^{o} C. The inhibition percentage was calculated, and SOD activity was expressed in U/ g. tissue. The antioxidant enzyme glutathione peroxidase (GPx) was determined according to the instructions of the kit from (Biodiagnostics, Cairo, Egypt). Briefly, 0.1 ml supernatant of 50% w/v kidney homogenate was mixed with 1 ml buffer (phosphate buffer, pH 7), 0.1 ml of NADPH reagent (glutathione, glutathione reductase and β-nictinamide-adinine dinucleotide phosphate reduced NADPH) and 0.1 ml of hydrogen peroxide (diluted 100 times before use). A decrease of the absorbance was recorded at 340 nm/min. The units of the enzyme activity were expressed as U/ g. tissue.

Processing of tissue samples and histopathology

Kidney tissue sections were fixed in 10% neutral-buffered formalin. The slides were dehydrated in gradient ethanol, cleared in xylene, embedded in paraffin blocks, sectioned in a thickness of 4 µm and then stained with hematoxylin (RICCA Chemical Co., TX, USA) and eosin (EMD Chemicals, NJ, USA).

Immunohistochemistry evaluation

The serial sections were dewaxed, hydrated, and immersed in an antigen retrieval (EDTA solution, pH 8). They were then treated with hydrogen peroxide 0.3% in methanol for 15 min and protein blocker for 30 min (to block the endogenous peroxidase activity and non-specific binding sites respectively), followed by incubation with rabbit anti-iNOS polyclonal antibody for 32 min. The sections were then counterstained with Mayer's hematoxylin. The slides were rinsed three times with PBS, incubated with anti-rabbit IgG secondary for 30 minutes at room temperature, visualized with di-aminobenzidine commercial kits and finally

counterstained with Mayer's haematoxylin. As a negative control procedure, the primary antibody was replaced by normal mouse serum. The labelling index of iNOS was expressed as the percentage of the positive area per total area in 8 high power fields (Saber et al. 2019).

Statistical Analysis

All values were presented as means ± standard error of the means (SEM). Statistical analysis was performed using Graph Pad Prism version 5 (Graph Pad, San Diego, CA, USA). Comparison between groups was carried out using one-way analysis of variance (ANOVA), followed by the post-hoc dunett test to analyse the data. Difference was considered significant when $p< 0.05$.

Identification of the phytochemical constituents:

Flavonoids:

Peak 5 and 8 with precursor ions at [M-H] *m/z* 637 and *m/z* 621 respectively showed base peak at *m/z* 351 (M-H-aglycone) corresponding to dihexuronide moiety. They were identified as luteolin-7-*O*-dihexuronide and apigenin -7-*O*-dihexuronide respectively (Quirantes-Piné et al. 2009)(Gong et al. 2016). Peaks 12 and 14 showed deprotonated molecular ion at *m/z* 623 and *m/z* 607, respectively. They exhibited two sequential losses of hexose moiety (162 amu) followed by hexuronide moiety (176 amu). They were tentatively identified as luteolin-7-*O*-hexosyl (1-2) hexuronide and apigenin-7-*O*-hexosyl (1-2) hexuronide respectively. Peak 15, 17 and 18 having deprotonated molecular ion at $[M-H]^-$ *m/z* 461, *m/z* 445 and *m/z* 475, respectively, showed a loss of 176 amu corresponding to hexuronide moiety to give a major fragment at 285, 269 and 299 respectively. They were tentatively identified as luteolin-7-*O*- hexuronide, apigenin-7-*O*- hexuronide and hespidulin-7-O- hexuronide (Gong et al. 2016)(Ana Plazonić et al. 2009)(Abdel-hady et al. 2018).

Peak 16 exhibited a precursor ion at *m/z* 593 with four consecutive losses, two of 90 amu leading to formation of products ions at *m/z* 503 $(M-H-90)^-$ and 383$(M-H-90-90)^-$, and two of 120 amu leading to product ions at *m/z* 473$(M-H-120)^-$ and 353$(M-H-120-120)^-$. This fragmentation pathway is usually observed in C-glycosylated flavonoids. It was tentatively identified as apigenin-6,8-di-C-glucoside (vicenin-2) (Friscic et al. 2016).

Each of the peaks 31, 32 and 33 exhibited a deprotonated molecular ion at *m/z* 431, *m/z* 447 and *m/z* 449, respectively, and gave a major loss of 162 amu, which was attributed to hexose residue. They were identified as apigenin hexoside, luteolin hexoside and eriodictyol

hexoside (Ana Plazonić et al. 2009)(Guimarães et al. 2013). Peak 35 showed [M-H] at *m/z* 593 with a major loss of 308 amu attributed to rutinoside residue. It was identified as luteolin rutinoside (Ana Plazonić et al. 2009).

Presence of luteolin (peak 36) and apigenin (peak 38) was confirmed by comparing their UV and mass spectral data to previous published data (Friscic et al. 2016).

Phenylethanoid glycosides

Peak 23 and 24 showed $[M-H]^-$ ion at *m/z* 623. It initially lost 162 amu that was attributed to the neutral loss of caffoeyl moiety to give the product ion *m/z* 461 $(M-H\text{-caffoeyl})^-$. A further loss of 146 amu gave the fragmented ion at *m/z* 315 $(M-H\text{-deoxyhexose})^-$ which was attributed to the loss of deoxyhexose moiety from the ion at *m/z* 461. The cleavage of the caffoeyl moiety produced the diagnostic ions at *m/z* 179. They were unambiguously identified as verbascoside (acteoside) and isoverbascoside (isoacteoside) (Li et al. 2014).

Peak 6 exhibited a precursor ion at *m/z* 461. It lost 146 amu to give *m/z* 315 (M-H-deoxyhexose). A further loss of 180 amu resulted in the product ion at *m/z* 135 $(M-H\text{-deoxyhexose-glucose})^-$ which corresponds to the phenylethanoid moiety. This compound was identified as a possible degradation product of verbascoside, namely decaffoeyl verbascoside or verbasoside (Quirantes-Piné et al. 2009).

Peak 19 and 26 showed precursor ions at *m/z* 785 and *m/z* 769. These compounds were identified as verbascoside derivatives with an additional hexose and deoxyhexose moieties respectively. They were identified as rossicaside A and poliumoside respectively (Friscic et al. 2016)(Abdel-hady et al. 2018). Peak 20 showed a precursor ion at *m/z* 801. The product ion at *m/z* 639 $(M-H-162)^-$ was attributed to the loss of hexose moiety which upon further loss of water molecule produced the base peak at *m/z* 621(suspensaside A) $(M-H-162-18)^-$. It was tentatively identified as suspensaside hexoside. Peak 21 with $[M-H]^-$ ion at *m/z* 639 showed a base peak at *m/z* 621 indicating an easy loss of hydroxyl moiety. This suggested that OH group was on the β-position of phenylethyl group. Fragments were observed at *m/z* 487, 459 and 179 showing a very similar pattern to that of suspensaside A, so the ion at *m/z* 621 might be suspensaside A and this compound (*m/z* 639) was tentatively identified as suspensaside (Han et al. 2007).

Peak 22 with $[M-H]^-$ ion at *m/z* 621 gave a diagnostic ion at *m/z* 487 $(M-H-134)^-$ which was attributed to the cleavage of six-member ether ring accompanying H

transformation. The fragmented ion at *m/z* 459 $(M-H-162)^-$ in addition to the fragment at *m/z* 179 suggested the presence of a caffoeyl group. The product ion at *m/z* 475 $(M-H-146)^-$ indicated the concurrent loss of deoxyhexose. These findings were in agreement with those reported on suspensaside A in a previous study (Han et al. 2007).

Peak 25 with $[M-H]^-$ ion at *m/z* 651 which is 28 amu more than verbascoside, indicates the presence of two methoxy groups on phenylethyl moiety. It yielded product ions at *m/z* 505 (M-H-deoxyhexose), 489 (M-H-caffoeyl) and 487 (M-H- phenylethanoid dimethyl ether). It was tentatively identified as brachynoside (Guo et al. 2007).

Peak 27 exhibited deprotonated molecular ion at *m/z* 667. It yielded a fragmented ion at *m/z* 621 $(M-H-46)^-$ due to the loss of hydroxy ethyl group. A further loss of 162 amu resulted in the product ion at *m/z* 459 $(M-H-46\text{-caffoeyl})^-$. It was identified as β- ethyl-OH-verbascoside (Guo et al. 2007).

Peak 28 showed $[M-H]^-$ ion at *m/z* 607. Two distinctive fragment ions at *m/z* 461 $(M-H-146)^-$ and *m/z* 445 $(M-H-162)^-$ were attributed to hexose and deoxyhexose moieties loss. A further loss of 162 Da from *m/z* 461 or 146 Da from *m/z* 445 produced the fragmented ion at *m/z* 299 $(M-H-162-146)^-$ which consists of the remaining glucose moiety (162 amu) and phenylethanoid moiety with only one hydroxyl group (137 amu). The presence of the fragment *m/z* 179 confirmed the caffeic acid existence. It was tentatively identified as dehydroxy verbascoside.

Peak 29 having $[M-H]^-$ ion at *m/z* 637 showed a base peak at 461 $(M-H-176)^-$ and a fragment ion at *m/z* 193 that confirmed the presence of a feruloyl moiety. The product ion at *m/z* 315 $(M-H-176-146)^-$ was attributed to the loss of deoxyhexose from *m/z* 461. This compound was identified as leucosceptoside A (Li et al. 2014).

Peak 30 with precursor ion at *m/z* 665 generated a product ion at *m/z* 623 due to the loss of acetyl moiety (42 amu). The fragmentation pattern 623, 461,443 and 315 is similar to that of verbascoside. The compound was identified as 2'-acetyl verbascoside (Gong et al. 2016).

Iridoid glycosides

Peak 2 and 7 showed precursor ion at *m/z* 389. They both showed loss of 162 amu to give the aglycone at *m/z* 227 (M-H-hexose). The MS3 fragmentation was characterized by *m/z* 209 (M-H-162-18), *m/z* 191(M-H-162-18-18) and *m/z* 165(M-H-162-18-44). The base peak of

compound 32 was at *m/z* 209 while the base peak of compound 35 is at *m/z* 345. Compound 32 and 35 were identified as deacetyl asperulosidic acid and theveside respectively. The differentiation between them was based on their different retention times and base peak compared to the previous reported compounds (Zhao et al. 2018)(Quirantes-Piné et al. 2009).

Peak 4 with $[M-H]^-$ ion at *m/z* 373 produced a base peak at *m/z* 211 (aglycone) due to neutral loss of 162 amu (hexose). The loss of water and CO_2 due to MS_3 fragmentation resulted in *m/z* 167, *m/z* 149 and *m/z* 123 fragments. It was identified as geniposidic acid (Quirantes-Piné et al. 2009).

Phenolic acids and other polar compounds

Peaks 1, 9 (*m/z* 341) and 13(*m/z* 325) exhibited major loss of 162 amu (hexose moiety). Compounds 1 and 9 gave two distinctive peaks at *m/z* 179 and *m/z* 161 characteristic to caffeic acid and were identified as caffeic acid hexoside (Friscic et al. 2016). Compound 13 showed major fragmented ions at *m/z* 163, *m/z* 145 and *m/z* 119 characteristic to coumaric acid and was identified as coumaric acid hexoside (Friscic et al. 2016). Peak 11(*m/z* 487) showed two consecutive losses of 146 amu and 162 amu to give the base peak at *m/z* 179. Peak 3 (*m/z* 165) gave major fragment at *m/z* 121 and was identified as phloretic acid (Allen et al. 2015). Compound 11 was identified as caffeic rutinoside (cistaniside F) (Gong et al. 2016).

Peak 10 (*m/z* 387) showed a base peak at *m/z* 207 $(M-H\text{-hexose-}\ H_2O)^-$ and fragmented ions at *m/z* 225 $(M-H\text{-hexose})^-$ and *m/z* 163 $(M-H\text{-hexose-}\ H_2O\text{-}\ CO_2)^-$. It was tentatively identified as tuberonic acid hexoside (Gong et al. 2016).

Oxygenated fatty acids

Peaks 37 (m/z 329) and 34 (m/z 327) showed a mass difference of 2 amu indicating the presence of an extra double bond. They were tentatively identified as trihydroxyoctadecadienoic acid and trihydroxyoctadecaenoic acid (Farag et al. 2016 and Otify et al. 2015).

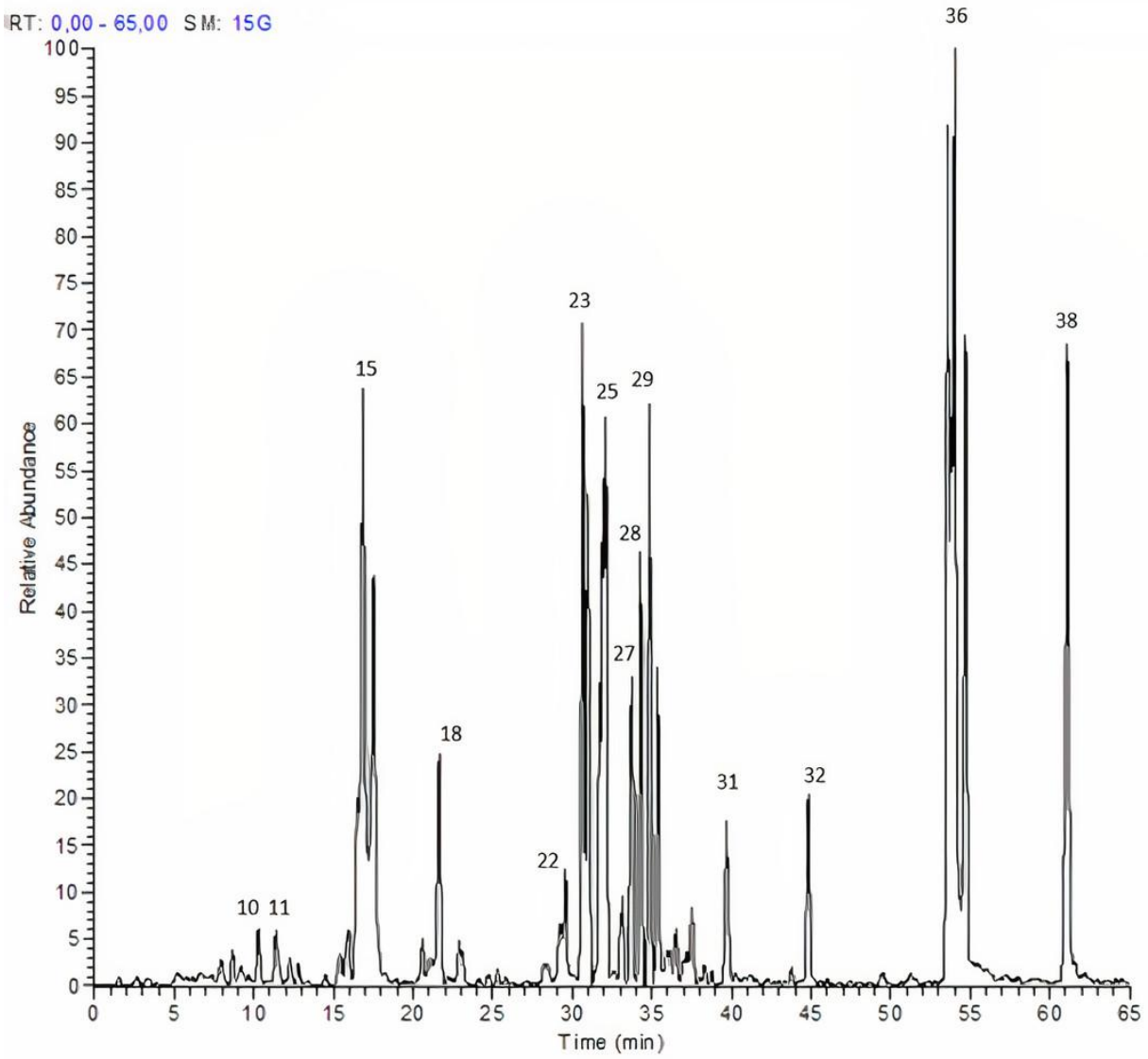

Figure S1. LC-MS profile of *L. camara* L. flowers extract in negative mode.

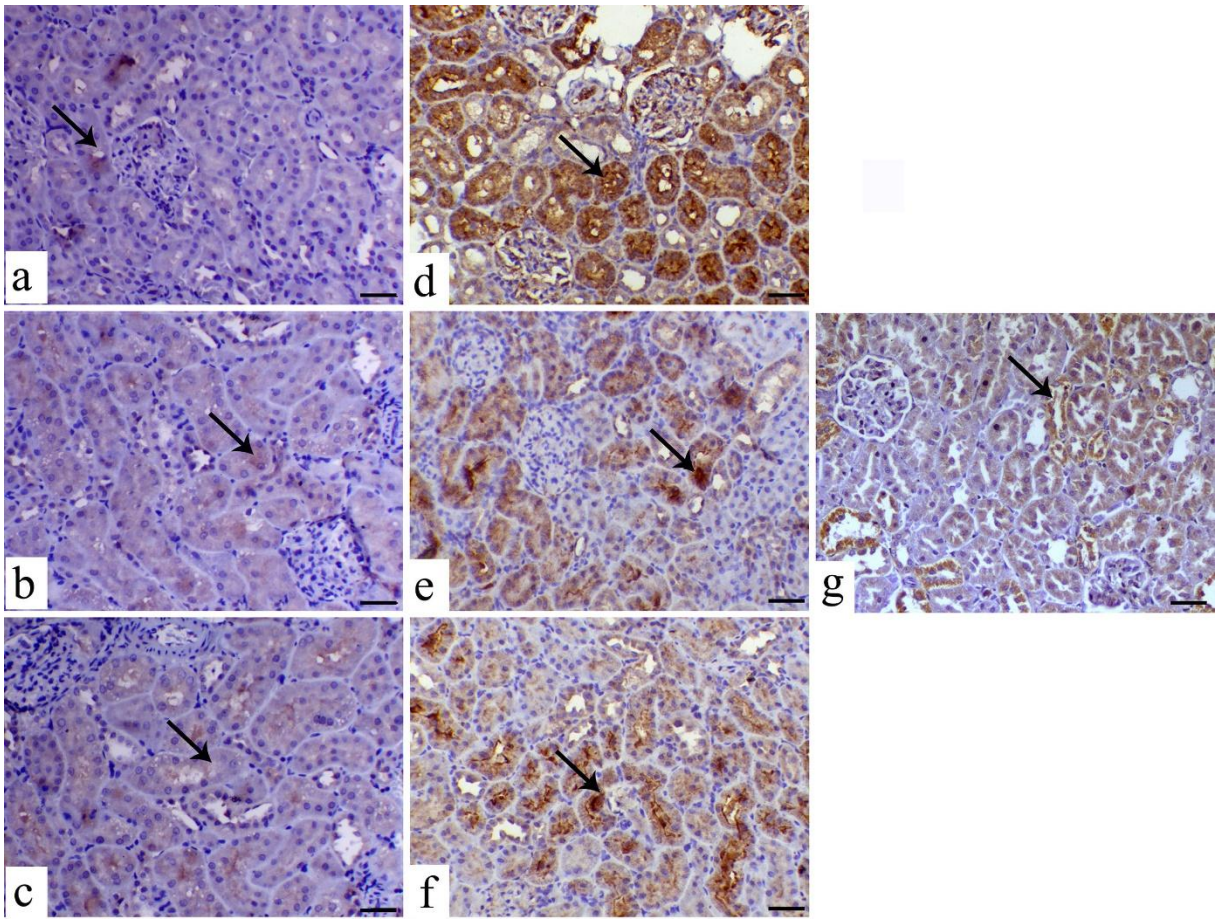

Figure S2. Photomicrograph of kidneys showing marked iNOS expression within the renal tubular epithelium (arrow), bar = 50 µm.

a: control saline; b: flowers extract (400 mg/kg b.wt); c: cystone (400 mg/kg b.wt); d: control positive animal (EG) ; e: EG + flowers extract (200 mg/kg b.wt); f: EG + flowers extract (400 mg/kg b.wt); g: EG + cystone (400 mg/kg b.wt)

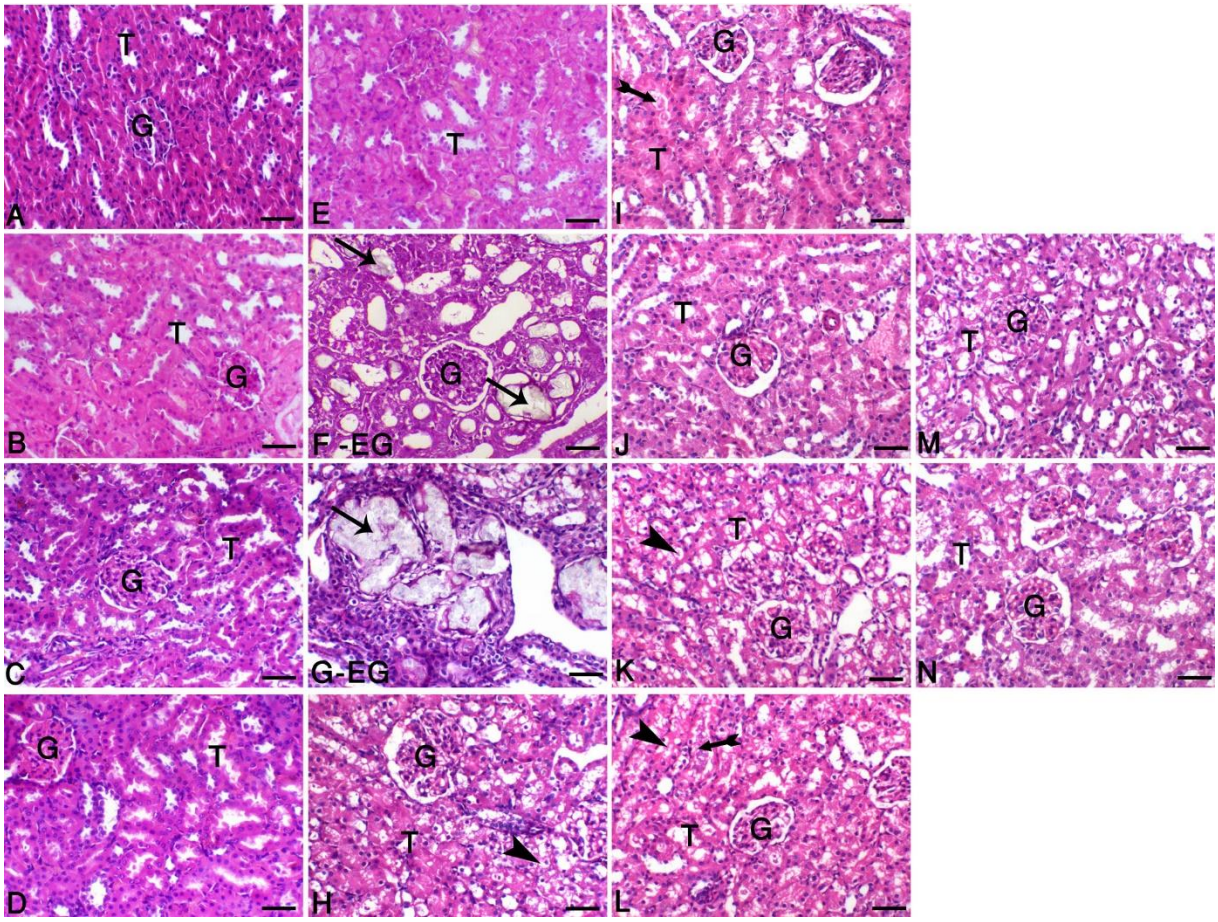

Figure S3. Photomicrograph of kidneys from different treated groups.

A: control saline; B: control cystone; C: flowers extract (400 mg/kg b.wt). D: roots extract (400 mg/kg b.wt); E: leaves extract (400 mg/kg b.wt); F and G: the ethylene glycol. H and I: EG-+ flower extract at 200 and 400 mg/kg b.wt. respectively; J: EG+ cystone. K and L: EG + roots extract at 200 and 400 mg mg/kg b.wt. respectively; M and N: EG+ leaves extract at 200 and 400 mg/kg b.wt respectively; G: renal glomeruli; T: renal tubules. Arrows reveal Ca oxalate crystal within the lumen of the renal tubules. Arrowheads indicate vacuolar degeneration within renal tubules and tailed arrows indicate protein cast, H&E, bar= 50 µm.

Table S1. Identified metabolites in *L. camara* L. flower extract using HPLC-PDA-ESI-MS/MS in negative mode.

No	Rt (min)	λ_{max} (nm)	$(M-H)^-$	Mass fragmentation	Identified compounds	Class of compounds	Ref.
1	1.68	235	341	215,179,161	Caffeic acid hexoside [c]	Phenolic acid	(Friscic et al. 2016)
2	3.18	226	389	345,209,191,147	Deacetyl asperulosidic acid [c]	Iridoid glycosides	(Zhou et al. 2010)
3	3.92	278	165	121	Phloretic acid [c]	Phenolic acid	(Allen et al. 2015)
4	4.13	285	373	311,211,167,149, 123	Geniposidic acid [c]	Iridoid glycosides	(Fu et al. 2014)
5	5.21	217,289	637	461,351,285,193	Luteolin-*O*-dihexuronide [a]	Flavonoids	(Quirantes-Piné et al. 2009) (El-Kassem et al. 2015)
6	6.59	268	461	443,315,161,135	Verbasoside (decaffoeyl verbascoside) [a]	Phenylethanoid glycosides	(Quirantes-Piné et al. 2009) (Abdel-hady et al. 2018)
7	7.00	267,325	389	345, 209,165,121	Theveside [a]	Iridoid glycosides	(Quirantes-Piné et al. 2009) (Clive W Ford & M Robin Bendall 1980)
8	7.72	267,323	621	487,351,269,193	Apigenin-*O*-dihexuronide [a]	Flavonoids	(Gong et al. 2016) (El-Kassem et al. 2015)
9	8.68	297,320	341	281,179,161,135	Caffeic acid hexoside [c]	Phenolic acids	(Friscic et al. 2016)
10	10.31	246,299, 324	387	369,207,163,119	Tuberonic acid hexoside [a]	Monocarboxylic acid	(Abdel-hady et al. 2018)
11	11.87	248	487	341,179	Cistaniside F (caffeic rutinoside) [c]	Phenolic acid	(Gong et al. 2016)
12	12.85	261,311	623	461,443,285	Luteolin-7-*O*-hexosyl(1-2) hexuronide [c].	Flavonoids	
13	13.08	281	325	163,145,119	coumaric acid hexoside [c]	Phenolic acid	(Friscic et al. 2016)
14	15.31	265, 324	607	445,337, 269,225	Apigenin-7-*O*-hexosyl(1-2) hexuronide [c]	Flavonoids	
15	16.85	266,288, 335	461	285,175	Luteolin-O-hexuronide [a]	Flavonids	(Gong et al. 2016) (El-Kassem et al. 2015)
16	20.78	267, 326	593	575,503,473,383, 353	Vicenin -2 (Apigenin-6,8-C-diglucoside) [a]	Flavonoids	(Friscic et al. 2016) (Abdel-hady et al. 2018)
17	21.64	269, 315	445	269,175	Apigenin- 7- *O*- hexuronide [a]	Flavonoids	(Friscic et al. 2016) (El-Kassem et al. 2015)
18	22.90	286, 330	475	299,284,175,161	Hispidulin-7-*O*- hexuronide [a]	Flavonoids	(Abdel-hady et al. 2018)
19	23.09	327	785	623,461,443	Rossicaside A [c]	Phenylethanoid glycosides	(Friscic et al. 2016)
20	24.08	308	801	741,711,639,621, 341	Suspensaside hexoside [c]	Phenylethanoid glycosides	
21	24.64	220, 308	639	621,529,477,459,	Suspensaside [c]	Phenylethanoid	(Han et al. 2007)

				179		glycosides	
22	29.58	219, 319	621	487,475,459,179	Suspensaside A [a]	Phenylethanoid glycosides	(Han et al. 2007) (Abdel-hady et al. 2018)
23	30.66	329	623	461,315,179	Verbascoside [a]	Phenylethanoid glycosides	(Li et al. 2014) (Taoubi et al. 1997)
24	31.59	329	623	461,315,179	Isoverbascoside [a]	Phenylethanoid glycosides	(Li et al. 2014) (Taoubi et al. 1997)
25	32.49	328	651	505,489,487,325	Brachynoside [c]	Phenylethanoid glycosides	(Guo et al. 2007)
26	32.56	327	769	623,607 ,461	Poliumoside [a]	Phenylethanoid glycosides	(Abdel-hady et al. 2018)
27	33.99	328	667	621,487,459	*β*- ethyl-OH- verbascoside [c]	Phenylethanoid glycosides	(Li et al. 2014)
28	34.87	327	607	461,445,427,299, 179	Dehydroxy verbascoside [c]	Phenylethanoid glycosides	
29	35.38	316	637	475,461,443,315, 193	Leucosceptoside A [c]	Phenylethanoid glycosides	(Li et al. 2014)
30	38.27	323	665	623,503,461,443, 315	2'-acetyl verbascoside [c]	Phenylethanoid glycosides	(Gong et al. 2016)
31	39.68	329	431	269	Apigenin-7-*O*- hexoside [a]	Flavonoids	(Ana Plazonić et al. 2009) (El-Kassem et al. 2015)
32	44.83	329	447	429,285,179	Luteolin -7-*O*-hexoside [a]	Flavonoids	(Ana Plazonić et al. 2009) (El-Kassem et al. 2015)
33	48.31	289, 319	449	431,287	Eriodictyol-7-*O*- hexoside [c]	Flavonoids	(Guimarães et al. 2013)
34	50.23	272	327	309,291,239,229, 171	Trihydroxy-octadecadienoic acid [c]	Fatty acid	(Farag et al. 2016)
35	51.27	329	593	575,447,429,285	Luteolin-7-*O*- rutinoside [c]	Flavonoids	(Ana Plazonić et al. 2009)
36	54.01	269, 332	285	285,267,217	Luteolin [b]	Flavonoids	(Friscic et al. 2016) (Wollenweber et al. 1997)
37	54.72	274	329	329,311,293,229, 171	Trihydroxy octadecenoic acid [c]	Fatty acid	(Otify et al. 2015)
38	61.10	268, 332	269	269,225,149,107	Apigenin [b]	Flavonoids	(Friscic et al. 2016) (Nagao et al. 2002)

[a] previously reported in *L. camara*, [b] previously reported in *L.* genus, [c] reported for the first time in *L. camara*

Table S2. Effect of *L. camara* extracts (flowers, roots and leaves), ethylene glycol and their combination on serum calcium and oxidative stress markers in rat kidney homogenates.

	Calcium	**Creatinine**	**Urea**	**Uric acid**	**SOD**	**GPx**	**MDA**
Groups	mg/dl	mg/dl	mg/dl	mg/dl	**U/g tissue**	**U/g tissue**	**nmol/g tissue**
Group I (Saline)	5.27± 0.16	0.66± 0.1	26.29± 4.82	2.02± 0.33	285.8±11.58	33±3.1	5.23±0.79
Normal groups							
Group II (Cys.)	5.52± 0.33	0.73± 0.18	28.71± 4.68	1.91± 0.31	305±11.83	34.83±2.92	5.47±0.78
Group III (FlE 400)	5.42± 0.39	0.75± 0.18	24.57± 4.61	1.96± 0.36	386.3±10.23	37.17±3.54	5.57±0.64
Group IV (RE 400)	5.55± 0.24	0.71± 0.16	26.71± 4.38	1.96± 0.26	374.2±7.11	36.05±2.61	5.56±1.05
Group V (LE 400)	5.45± 0.21	0.73± 0.18	27.00± 5.89	1.89± 0.24	330.8±9.17	33.88±2.69	5.9±0.85
EG-induced urolithiatic groups							
Group VI (EG)	8.33^{a} ± 0.65	2.11^{a} ± 0.29	54.14^{a} ± 10.76	5.46^{a} ± 0.64	167.3^{a}±8.57	20.83^{a} ±1.72	16.77^{a} ±1.25
Group VII (EG + Cys.)	5.90^{b} ± 0.41	0.86^{b} ± 0.19	30.14^{b} ± 6.62	2.47^{b} ± 0.45	265^{b} ±17.89	$30^{a,b}$ ±3.28	6.52^{b} ±1.02
Group VIII (EG + FlE 200)	$6.07^{a,b}$ ± 0.40	$1.12^{a,b}$ ± 0.12	28.00^{b} ± 2.83	$3.78^{a,b}$ ± 0.74	$254.8^{a,b}$ ±14.29	$27.28^{a,b}$ ±2.34	$7.62^{a,b}$ ±1.06
Group IX (EG + FlE 400)	5.59^{b} ± 0.38	0.81^{b} ± 0.11	25.7^{b} ± 5.59	2.38^{b} ± 0.30	$324.2^{a,b}$ ±24.58	32.63^{b} ±2.06	6.35^{b} ±1.01
Group X (EG+RE 200)	$5.95^{a,b}$ ± 0.12	$1.05^{a,b}$ ± 0.11	$37.71^{a,b}$ ± 6.16	2.55^{b} ± 0.33	$215.8^{a,b}$ ±24.58	$28.12^{a,b}$ ±1.63	$9.9^{a,b}$ ±0.89
Group XI (EG+RE 400)	5.57^{b} ± 0.31	0.76^{b} ± 0.10	28.00^{b} ± 3.27	2.01^{b} ± 0.25	$310.5^{a,b}$ ±13.17	29.67^{b} ±2.24	$7.07^{a,b}$ ±1.27
Group XII (EG+LE 200)	$5.99^{a,b}$ ± 0.16	$0.99^{a,b}$ ± 0.14	$37.86^{a,b}$ ± 8.63	$2.78^{a,b}$ ± 0.13	$211.7^{a,b}$ ±28.58	$26.6^{a,b}$ ±2.45	$10.17^{a,b}$ ±0.93
Group XIII (EG+LE 400)	5.53^{b} ± 0.43	0.80^{b} ± 0.12	30.43^{b} ± 5.38	2.43^{b} ±0.27	290^{b} ±8.94	29.08^{b} ±1.65	$7.18^{a,b}$ ±0.94

Values are mean ± SD. n=7 ; [a] significantly different from the normal control group (I) $p<0.05$; [b] significantly different from EG group VI $p< 0.0001$(one-way ANOVA); EG: ethylene glycol; FLE: flowers extract; LE: leaves extract; RE: roots extract.

Table S3. Positive area percentage of iNOS immunostaining within the different tested groups.

Tested groups	**Positive area %**	**Tested groups**	**Positive area %**
Group I: Control	5.09 ± 2.0179	Group IV: Ethylene glycol (EG)	61.94 ± 6.67
Group II: FlE 400	7.059 ± 1.457	Group V: EG + FlE 200	38.687 ± 4.424
Group III: Cystone	6.002 ± 0.678	Group VI: EG +FlE 400	27.209 ± 4.55
		Group VII: EG + cystone	30.674 ± 4.985

References:

Abdel-hady H, El-sayed MM, Abdel-hady AA, Hashash MM, Abdel-hady AM, Aboushousha T, Abdel-hameed ES, Abdel- EE, Morsi EA, Abdel-hady A, Hashash M. 2018. Nephroprotective Activity of Methanolic Extract of *Lantana camara* and Squash (*Cucurbita pepo*) on Cisplatin-Induced Nephrotoxicity in Rats and Identification of Certain Chemical Constituents of Lantana camara by HPLC-ESI- MS Plant materials. 10(1):136–147.

Allen F, Greiner R, Wishart D. 2015. Competitive fragmentation modeling of ESI-MS/MS spectra for putative metabolite identification. Metabolomics .11(1):98–110.

Ana Plazonić, Bucar F, Maleŝ Žeљan, Mornar A, Nigović B, Kujundžić N. 2009. Identification and quantification of flavonoids and phenolic acids in burr parsley (*Caucalis platycarpos* L.), using high-performance liquid chromatography with diode array detection and electrospray ionization mass spectrometry. Molecules. 14(7):2466–2490.

Bora KS, Singh B. 2019. Evaluation of antiepileptic activity of *Lantana camara* (Linn.) flowers in Swiss albino mice. TJPS. 43(4):195–200.

Clive W Ford, M Robin Bendall. 1980. Identification of the Iridoid Glucoside Theveside in *Lantana camara* (Verbenaceae), and Determination of its Structure and stereochemistry by means of N.M.R. Aust jChem. 33:509–518.

El-Kassem LTA, Mohammed RS, Souda SS El, El-Anssary AA, Hawas UW, Mohmoud K, Farrag ARH. 2015. Digalacturonide Flavones from Egyptian *Lantana camara* Flowers with in vitro Antioxidant and in vivo Hepatoprotective Activities. Zeitschrift für Naturforsch C. 67(7–8):381–390.

Farag MA, Rasheed DM, Kropf M, Heiss AG. 2016. Metabolite profiling in *Trigonella* seeds via UPLC-MS and GC-MS analyzed using multivariate data analyses. Anal Bioanal Chem. 408(28):8065–8078.

Friscic M, Bucar F, Hazler K. 2016. LC-PDA-ESI-MS n analysis of phenolic and iridoid compounds from *Globularia* spp . Mass Spectrom. 51:1211–1236.

Fu Z, Xue R, Li Z, Chen M, Sun Z. 2014. Fragmentation patterns study of iridoid glycosides in *Fructus Gardeniae* by HPLC-Q / TOF-MS / MS. Biomed Chromatogr. 28:1795–1807.

Ghareeb MA, Sobeh M, El-maadawy WH, Mohammed HS. 2019. Chemical Profiling of Polyphenolics in *Eucalyptus globulus* and Evaluation of Its Hepato – Renal Protective

Potential Against Cyclophosphamide Induced Toxicity in Mice. Antioxidants. 8 (415):1-19.

Gong J, Miao H, Sun X, Hou W, Chen J, Xie Z, Liao Q. 2016. Simultaneous qualitative and quantitative determination of phenylethanoid glycosides and flavanoid compounds in *Callicarpa kwangtungensis* Chun by HPLC-ESI-IT-TOF-MS/MS coupled with HPLC-DAD. Anal Methods. 6:120–122.

Guimarães R, Barros L, Carvalho AM, Queiroz MJRP, Santos-buelga C, Ferreira ICFR. 2013. Characterization of Phenolic Compounds in Wild Fruits from Northeastern Portugal. Food Chem. 141(4):3721–3730.

Guo H, Liu A-H, Yang M, Guo D-A. 2007. Characterization of phenolic compounds in the fruits of *Forsythia suspensa* by high-performance liquid chromatography coupled with electrospray ionization tandem mass spectrometry. Rapid Commun Mass Spectrom. 21:715–729.

Han J, Ye M, Guo H, Yang M, Wang B rong, Guo D an. 2007. Analysis of multiple constituents in a Chinese herbal preparation Shuang-Huang-Lian oral liquid by HPLC-DAD-ESI-MSn. J Pharm Biomed Anal. 44(2):430–438.

Li C, Liu Y, Abdulla R, Aisa HA, Suo Y. 2014. Determination of Phenylethanoid Glycosides in *Lagotis brevituba* Maxim. by High-Performance Liquid Chromatography-Electrospray Ionization Tandem Mass Spectrometry. Anal Lett. 47(11):1862–1873.

Nagao T, Abe F, Kinjo J, Okabe H. 2002. Antiproliferative constituents in plants 10. Flavones from the leaves of *Lantana montevidensis* Briq. and consideration of structure-activity relationship. Biol Pharm Bull. 25(7):875–9.

Otify A, George C, Elsayed A, Farag MA. 2015. Mechanistic evidence of *Passiflora edulis* (Passifloraceae) anxiolytic activity in relation to its metabolite fingerprint as revealed via LC-MS and chemometrics. Food Funct. 6(12):3807–3817.

Quirantes-Piné R, Funes L, Micol V, Segura-Carretero A, Fernández-Gutiérrez A. 2009. High-performance liquid chromatography with diode array detection coupled to electrospray time-of-flight and ion-trap tandem mass spectrometry to identify phenolic compounds from a *Lemon verbena* extract. J Chromatogr A. 1216(28):5391–5397.

Saber S, Khalil RM, Abdo WS, Nassif D, El-ahwany E. 2019. Olmesartan ameliorates chemically-induced ulcerative colitis in rats via modulating NF κ B and Nrf-2 / HO-1

signaling crosstalk. Toxicol Appl Pharmacol. 364:120–132.

Taoubi K, Fauvel MT, Gleye J, C.Moulis, I.Fouraste. 1997. Phenylpropanoid Glycosides from *Lantana camara* and *Lippia multiflora*. Planta Med. 63(1 997):192–193.

Wollenweber E, Dorr M, Siems K, Station E. 1997. Flavonoid Aglycones and Triterpenoids from the Leaf Exudate of *Lantana camara* and *Lantana montevidensis.* 1978(3):269–270.

Zhao X, Wei J, Yang M. 2018. Simultaneous analysis of iridoid glycosides and anthraquinones in *Morinda officinalis* using UPLC-QqQ-MS/MS and UPLC-Q/TOF-MSE. Molecules. 23(5).

Zhou T, Liu H, Wen J, Guorong Fan, Chai Y, Wu Y. 2010. Fragmentation study of iridoid glycosides including epimers by liquid chromatography-diode array detection/ electrospray ionization mass spectrometry and its application in metabolic fingerprint analysis of *Gardenia jasminoides* Ellis. Rapid Commun Mass Spectrom. 24:2520–2528.